Molten Salt Corrosion of Stainless Steels and Low-Cr Steel in CSP Plants

A. G. Fernández · M. I. Lasanta · F. J. Pérez

Abstract The corrosive effects of 60 % $NaNO_3$/40 % $NaNO_3$ have been tested at 390 and 550 °C, in order to simulate the working conditions in two principal concentrated solar power (CSP) plants, on stainless steel (AISI 304, 430) and on a low-Cr alloy steel (T22) containing 2.25 % Cr. The corrosion rates were determined by gravimetric tests, measuring the weight gain during 2,000 h, identifying the corrosion products via scanning electron microscopy (SEM) and X-ray diffraction (XRD). Thereby, Fe_2O_3 and Fe_3O_4 were the most prominent products formed from the tests performed at 390 °C, being observed also the formation of some stable compounds due to the impurities of the salt, as magnesium ferrite ($MgFe_2O_4$) and $NaFeO_2$. The study at 550 °C of stainless steels revealed a better behavior under corrosive environments than T22 steel, identifying the formation of $FeCr_2O_4$ protective spinels mainly. To complete the corrosion tests, thermo-physical studies were carried out in binary mixture, using DSC and TGA. Also the most important parameters of the salt before and after corrosion test were tested.

Introduction

Different kind of mixtures of alkali nitrates have been used as energy storage fluid in solar power during the last years. The most optimized mixture is called solar salt, and is composed by 60 % $NaNO_3$/40 % KNO_3. This mixture melts at 223 °C, is thermally stable about 600 °C, and offer a favourable combination of high density, low vapour pressure, moderate specific heat, low chemical reactivity, and low cost [1].

Molten nitrate mixture must also satisfy another important requirements in solar plants, like thermal conductivity, diffusivity and a lower heat loss coefficient [2]. In order to increase the efficiency, the heat storage fluid needs to have a low vapor pressure for optimize the heat exchanging process. In this terms the solar power heat exchangers reaches 20 bar pressure and this can mean that heat losses occur.

The 60 % $NaNO_3$/40 % KNO_3 salt mixture is currently being used in two main types of concentrating solar power plants. The difference between them lies in the way of they concentrate solar radiation, which can be done using parabolic trough or central receiver tower [3].

The aim of this investigation is the study of the corrosion caused by the solar salt in different stainless steels and in low % Cr steel in a work temperature of those CPS plants, 390 and 550 °C.

Solar Tower Plant

This type of solar plants uses direct energy storage, resulting that heat transport fluid and the heat transfer fluid (HTF) are the same molten salts. The liquid salt at 290 °C is pumped from a ‘cold’ storage tank through the receiver which is heated until it reaches 565 °C, returning after to a ‘hot’ tank for its storage [3].

Hot salt is pumped to a steam generating system that produces superheated steam for a conventional cycle turbine system when power is needed from the plant and returned to the cold tank where it is stored and eventually reheated in the receiver to

avoid the freezing (Fig. 1).

Parabolic Trough Solar Power Plants

These plants are endowed with an indirect energy storage system which consists, like in the direct system, in two tanks but where the energy is stored though a second

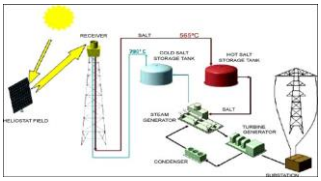

Fig. 1 Scheme of installation of a solar power tower, with two-tanks storage system

heat fluid (generally oil), not directly by the HTF. Heat from the HTF is absorbed in the oil-to-salt heat exchanger by the 60 % $NaNO_3$/40 % KNO_3 molten salts. The HTF is heated up at 390 °C and circulates through the collectors returning to a series of heat exchangers in the power block [4]. Figure 2 shows the flow process for a typical parabolic trough solar power plant with a two-tank molten salt storage.

In this solar power plant, when the storage system is discharged, salt from the hot storage tank is sent back to salt heat exchanger and is used to heat cold HTF again. The molten salt is then sent to the power plant and the cooled salt return to the cold storage tank where the temperature is about 300 °C.

The high freezing point (220 °C) of the molten salt is the major challenge to supervise in these compounds because is mandatory to ensure that the salt do not freeze in the solar field during the night or into the piping in lower temperature zones.

Corrosion Ability in These Salts

Corrosion can take place along mass transfer due to thermal gradient in the melt. This corrosion mode involves dissolution of an alloying element at hot spots and deposition of those elements in cooler spots. This may trigger into severe fouling and plugging in a circulating system. Corrosion is also strongly dependent on temperature and flux velocity of the salts and can appear like uniform, pitting or intergranular attack. In general, molten salt corrosion is quite similar to aqueous corrosion [7]

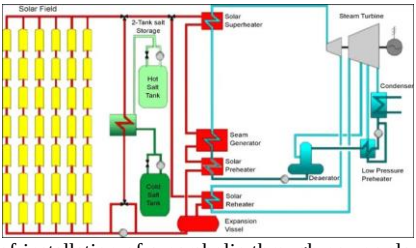

Fig. 2 Scheme of installation of a parabolic through power plant, with two-tanks

This degradation process occurs when a salt or salt mixture is being deposited or condensed over the metallic material. The corrosive attack is accelerated when the system's components reach temperatures of melting salt deposit, leading the

formation of a stable ionic electrolyte at elevated temperature, which holds a fluxing action over the protective layer fostering dissolution and transportation of oxidizing species to the metal and metal ions into the salt, thereby starting the phase of attack.

The corrosive effect of these salts is based on the following reduction reaction:

$$NO_3^- + 2e^- \rightarrow NO_2^- + O^{2-} \quad (1)$$

That results in oxidation of iron atoms which diffuse from the material [8]:

$$Fe + O^{2-} \rightarrow FeO + 2e^- \quad (2)$$

$$3FeO + O^{2-} \rightarrow Fe_3O_4 + 2e^- \quad (3)$$

In order to understand process in alkaline nitrates is important to point out the formation of different (several) oxide ions during the corrosion tests.

Experiences performed by I.B. Singh et al. [9, 10] indicate the existence of O^{2-} oxide, O_2^{2-} peroxide and O_2^- superoxide, arisen from unstable oxide ions in the nitrate melt.

As described through the following equations:

$$O^{2-} + NO_3^- \rightarrow NO_2^- + O_2^{2-} \quad (4)$$

$$O_2^{2-} + 2NO_3^- \rightarrow 2NO_2^- + 2O^- \quad (5)$$

Several authors have been studied the formation of those oxides in corrosive process in those salts [11–13], sustaining the formation of Na_2O and KO_2, whose ions K^+ and Na^+ have different affinities for the formed ions on the equations 1 and 5, as following:

$$2Na^+ + O^{2-} \rightarrow Na_2O \quad (6)$$

$$2K^+ + 2\,O_2^- \rightarrow KO_2 \quad (7)$$

The formation of those oxide hiders the electronic movement required for generate the cathodic reaction, decreasing the corrosive ability of the salt.

The moisture effect in those reactions is also studied by mentioned authors [12], establishing the following reaction intermedium:

$$H_2O + NO_3^- \rightarrow HONO_2 + OH^- \quad (8)$$

$$HONO_2 + 2e^- \rightarrow NO_2^- + OH^- \quad (9)$$

In this environment the oxides of potassium and sodium are more solvable allowing a better course of the cathodic reaction, increasing the corrosive ability of the salt.

$$H_2O + NO_3^- + 2e^- \rightarrow NO_2^- + 2\,OH^- \quad (10)$$

There are studies which have examined the behavior of materials in contact with 60 % $NaNO_3$ + 40 % KNO_3 to assess their application in solar power plants [8, 14].

As noted in these references, at temperatures between 250 and 500 °C, iron, mild steel and nickel alloys showed passivation characteristics in molten nitrate salt in agreement with thermodynamic considerations.

It is important to point out that the impurities present in some nitrates are able to generate insoluble compounds which increase the corrosion processes and can obstruct the pipes of solar power plants.

Bradshaw et al. [14] study the corrosion in $NaNO_3$/KNO_3 salt mixtures from diverse sources, analyzing only initial levels of chlorides, perchlorates, sulfates, and carbonates, and the concentration of nitrite.

.

Experimental Procedures

Thermal Analysis of Salts

Open platinum crucibles have been used in SDT Q600 calorimeter during thermal decomposition tests, in order to measure the weight variation on mixture along the temperature increasing.

In DSC Q20 equipment heating and cooling ramps at 10 °C/min have been performed showing the absorbed heat (endothermic peak) or emitted heat (exothermic peak) by the sample in each case. In order to obtain better sensibility on signals the aluminium crucibles are hermetically closed and the equipment is endowed with a refrigeration system for obtain major precision on the cooling curves.

The same mass must be kept on the crucibles in order to obtain a precise weigh measure and before start the test, is important to pre melt the salt with the aim of avoid weight changes due to a water losses.

This test is arranged using MDSC (Modulated differential scanning calorimeter), modulating the temperature 0.5 °C around 390 °C with 130 s period.

Both test (SDT and DSC) were performed in N_2 atmosphere and the mixture mass varies among 5 and 10 mg.

High Temperature Corrosion Study

The search for new materials is necessary due to substantial increase in the temperature of the new solar power plants and the aim of this research is to increase the average life of its constituent materials to improve the plant performance.

Along with the thermo-physic study of salts, the corrosion caused on steels have been evaluated. Table 1 shows the tested steels.

T22 is a heat-resistant alloy steel with a chromium content of 2.25 %, which is widely used in pipes and pipelines in industrial plants for power generation. AISI 304 is an austenitic stainless steel and AISI 430 is a ferritic steel with a similar content in Cr.

Table 1 Chemical compositions of the alloy samples

	Material		
	AISI 304	T22	AISI 430
Wt%			
Si	0.41	\ 0.50	0.4
Mn	1.76	0.30–0.60	0.2
Ni	8.04	–	0.18
Cu	0.32	–	0.03
Cr	18.28	1.90–2.60	16.21
P	0.029	0.30	0.018
Mo	0.27	0.87–1.13	0.01
Co	0.14	–	0.02
C	0.055	\ 0.15	0.044
S	0.001	0.30	0.002
N	0.0498	–	0.038
Sn	0.016	–	0.010
Ti	0.016	–	0.02
Nb	0.008	–	0.003

The corrosion test was carried out in alumina crucibles, containing 60 % $NaNO_3$/ 40 % KNO_3 and the specimens of these materials have dimensions of 20 × 10 × 2 mm, polished with #600 SiC abrasive papers, washed with distilled water and acetone. The isothermal immersion tests were analyzed by gravimetric analysis at 24, 48, 150, 350, 500, 750, 1000, 1250, 1500, 1750 and 2000 h, where two specimens of each alloy were removed from the nitrate mixtures for examination and analysis.

The samples were slowly cooled and were washed with hot distilled water to remove excess salt in which they are immersed.

Results

Thermo-Physical Study

Melting point and latent heat of molten salts were measured in DSC-Q20 and the thermo-gravimetric analysis in SDT-Q600 (Fig. 3), and a summary of data obtained in the integration of the peaks can be observed in Table 2.

In Fig. 3, we can observe the curves of the isolated components $NaNO_3$ and KNO_3 and the thermal analysis belonging to the binary mixture 60 % $NaNO_3$ + 40 % KNO_3.

Table 2 shows the melting points and the latent heat of fusion obtained in Fig. 3.

The first transition at 131 °C is due to a phase change on the saline mixture.

For understand this phase transition is necessary to study the phase diagram of the binary mixture showed on Fig. 4, as well as the behaviour of the (Na, K)NO_3 compounds individually.

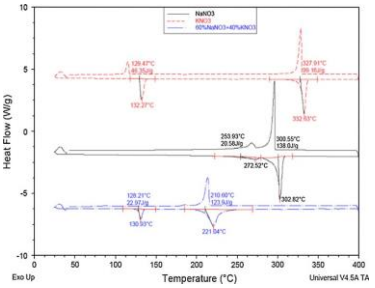

Fig. 3 DSC $NaNO_3$, KNO_3 and 60 % $NaNO_3$ + 40 % KNO_3 (Color figure online)

Table 2 Summary of data obtained in the integration of the peaks in Fig. 3

Mixtures	Integration temperature (°C)	DH_{fusion} (J/g)
KNO_3	332	99.16
$NaNO_3$	302.82	138
60 % $NaNO_3$ + 40 % KNO_3	221.04	123.9

Greis et al. [15] pointed in their work that sodium nitrate crystallizes in the space group $R\bar{3}c$ (a = 5.071 Å and c = 16.825 Å, hexagonal setting with Z = 6, at 25 °C, while potassium nitrate crystallizes in the space group Pmcn (a-KNO_3), aragonite type structure with a = 5.412 Å, b = 9.157 Å, c = 6.421 Å, Z = 4 at 25 °C. But in the heating ramp of the mixture 60 % $NaNO_3$ + 40 % KNO_3 the $R\bar{3}m$ solid solution (ss) (observed in this work at 131 °C) is formed by the two constituent phases, $NaNO_3$ and KNO_3 both having the same structure with space group $R\bar{3}m$.

The studies arranged by DSC on the components of sodium and potassium nitrate, show for $NaNO_3$, an slight phase transition at 272.52 °C assignable to the called *Landa transition*, where $NaNO_3$ change is internal order from $R\bar{3}c$ to take over the ss $R\bar{3}m$ and immediately afterwards melts at the temperature of 302 °C. By the other hand KNO_3, red curve in Fig. 3, shows $a \blacktriangle b$ phase transition at 132 °C, observing the fusion a 332 °C.

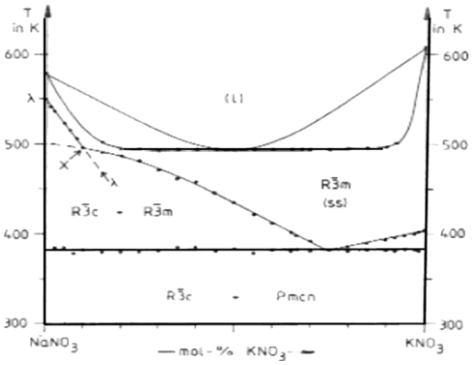

Fig. 4 60 % $NaNO_3$ + 40 % KNO_3 phase diagram

As noted in the works of Nimmo et al. [16], the structure of KNO_3 is:

- *a*-KNO_3 takes orthorhombic structure and space group Pmcn.
- *b*-KNO_3 takes R $\bar{3}$m and R $\bar{3}$c space group.
- *c*-KNO_3 takes R $\bar{3}$c group.

The heating of the mixture from room temperature leads a change from orthorhombic structure (*a*-KNO_3) to a trigonal structure (*b*-KNO_3), when 128 °C is reached.

Whereas we perform a cooling from 200 °C, KNO_3 changes to another trigonal phase *c*-KNO_3, among 124–100 °C, before rollback to *a*-KNO_3 phase.

At high temperature, *b*-KNO_3 must have major symmetry than *c*-KNO_3 phase enabling to assign to beta phase the R $\bar{3}$m space group.

The arising of the gamma new phase is possible due to the orientation of NO_3^- ions and their position. Each layer of NO_3^- lays among two layers of K and this disposal endow *c*-KNO_3 with ferroelectric properties.

As long as gamma structure is a single variation of beta phase, the reaching of beta structure is only possible via alpha phase. Note that if the beta structure will come from the heating of gamma starting from alpha, the arising reenrolment will be similar to the existing in *a* ◭ *b* transition.

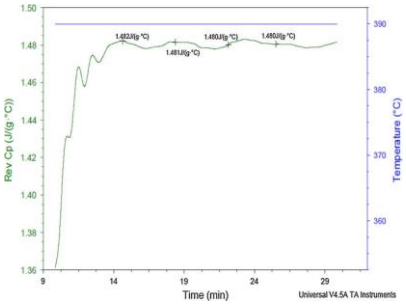

Fig. 5 C_p at 390 °C of 60 % $NaNO_3$ + 40 % KNO_3 mixture

In the tested binary mixture before this mentioned first transition, we reach the fusion at 221 °C.

Is important to emphasize the results in Table 2, where enthalpy of fusion of KNO_3 is less than $NaNO_3$, although sodium nitrate melts at lower temperature.

On the other hand the melting point in binary mixture is reduced and enthalpy has an intermediate value respect to the pure components.

Heat capacity and thermal stability are two important parameters to point out in these salts. High heat capacity is desirable because arises the use of less amount of salt in order to storage energy.

On the other hand high value of thermal stability leads the raising of the work temperature in the solar power plant.

The heat capacity obtained at 390 °C (Fig. 5) for the binary solar is 1.48 J/g °C, matching with the values given by Kearny et al. [17].

For the thermal stability tests (Fig. 6), the maximum levels of weight losses on the mixture was fixed on 3 %, taking this value as thermal stability limit of the salt, the maximum stability reached was 588.5 °C.

High Temperature Corrosion Results

The resume of the behavior of steels in saline 60 % $NaNO_3$/40 % KNO_3 at 390 °C for 2,000 h of gravimetric tests is shown in Fig. 7 for austenitic, ferritic and low chromium steels.

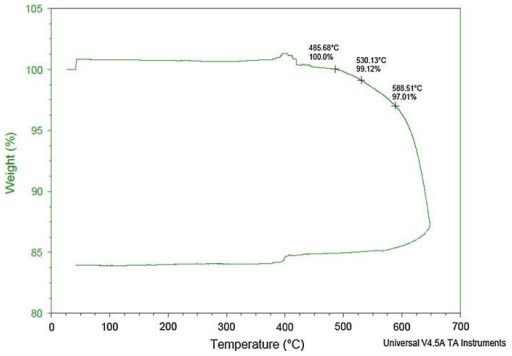

Fig. 6 TGA of 60 % $NaNO_3$ + 40 % KNO_3 mixture

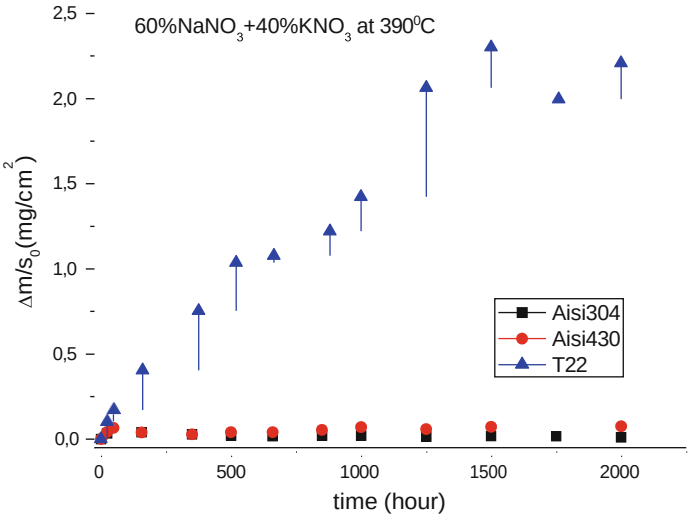

Fig. 7 Joint behavior of steels in saline 60 % $NaNO_3$ + 40 % KNO_3 at 390 °C for 2,000 h of test

Thus, T22 undergoes the greatest mass gain (2.25 mg/cm^2), as expected for a lower % Cr (2.25 %) steel, while the austenitic and ferritic steels have low mass gain, showing an optimal behaviour against corrosion, due to the higher content of

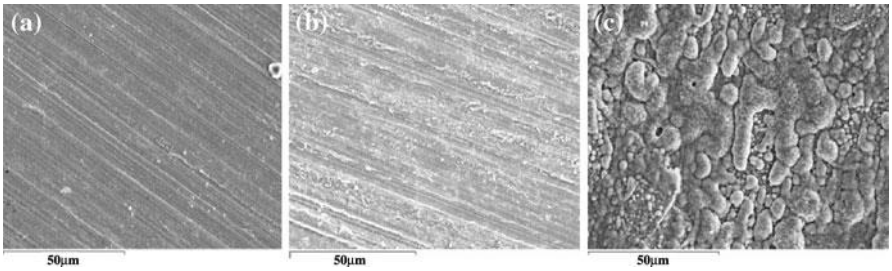

Fig. 8 Surface view of a AISI 304, b AISI 430 and c T22 after 2,000 h of test at 390 °C

Cr. This higher % Cr involves the prospect of the formation a protective layer of Cr_2O_3.

The no evidence of corrosion products in these steels, observed by scanning electron microscopy (SEM) (Fig. 8a, b) in superficial analysis for 2,000 h of immersion, reinforce the idea of the likelihood formation of this chromia protective layers; although this layers are not being detected experimentally.

On the other hand, T22 (Fig. 8c) steel suffer an important degradation on this surface, showing the formation of a porous oxide layers with several cracking allowing the diffusion of the salt and the corrosion of the base material. These results are consistent with the weight gain for those materials, shown in Fig. 7. Cross section of T22 steel is shown in Fig. 9.

In the outer zone (Fig. 9a) a less compact layer due to the formation of an oxide less adherent in this area (Fe_2O_3) has been detected. Closest to the base material more compact oxide layer of magnetite is found.

Abdel-Hakim et al. [18] has been suggested that Fe_2O_3 forms the external layer in contact with the salt, whereas Fe_3O_4 is the internal layer in contact with the metal

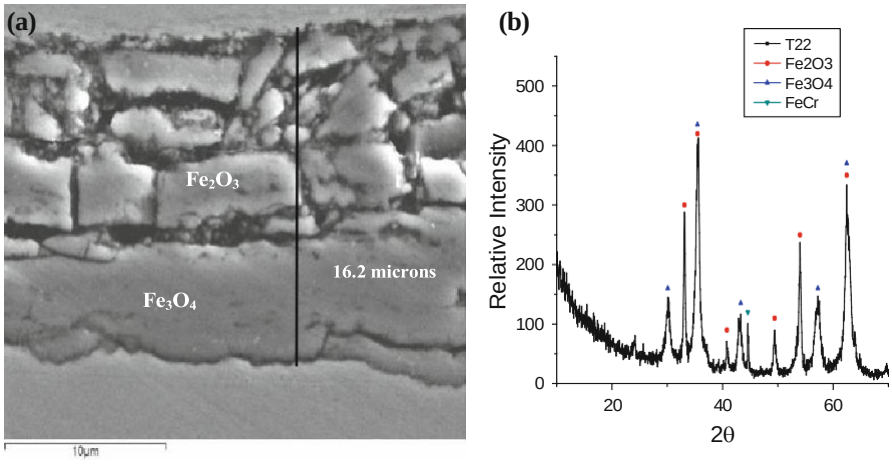

Fig. 9 a Cross section of T22 steel at the end of the test and b DRX

for steels exposed to a molten $NaNO_3$–KNO_3 eutectic mixture. This oxide Fe_2O_3 is an n-type conductor, which is susceptible to pitting corrosion.

The corrosion ranges on this binary mixture rises with the increasing of the temperature, from 390 to 550 °C.

These results, summarized in Figs. 10 and 11, reflect the general trends cited above for the stainless steels AISI 304 and 430.

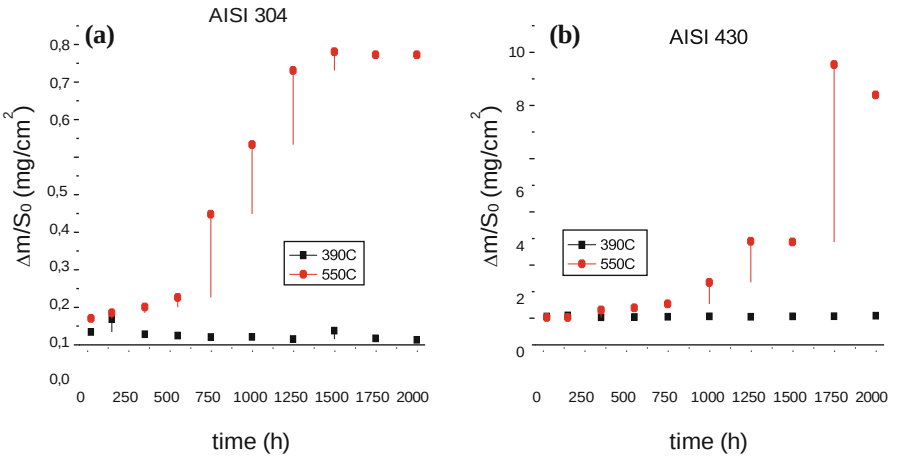

Fig. 10 Gravimetric comparison at 390 and 550 °C on a AISI 304 and b AISI 430

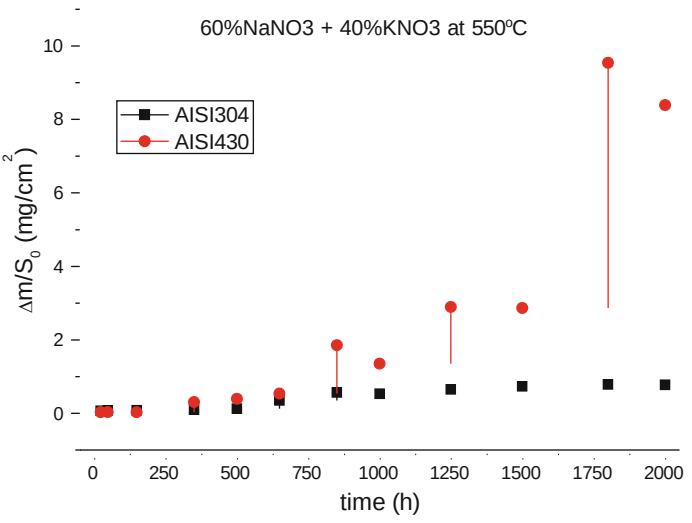

Fig. 11 Gravimetric analysis of stainless steels at 550 °C

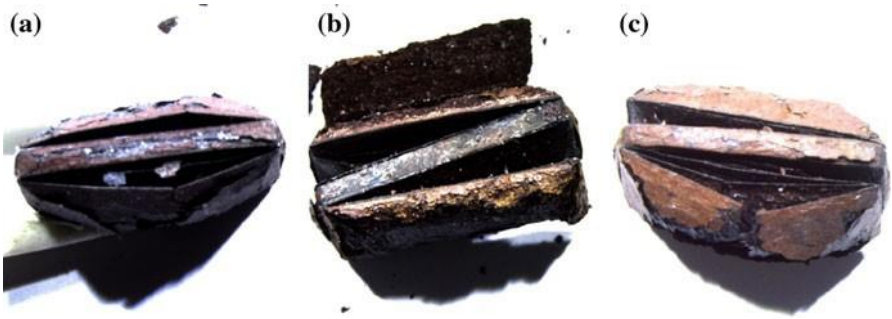

Fig. 12 Optical microscope images of T22 after a 350, b 500 and c 800 h of test

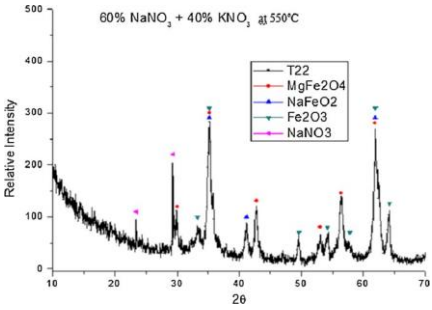

Fig. 13 DRX of T22 steel after 800 h of test

compounds with the impurities of the salt, as magnesium ferrite ($MgFe_2O_4$) and $NaFeO_2$.

In order to justify the results is important to review the basic behaviour of the binary salt [17] along the temperature is increasing.

In strongly basic media, $Fe_2O_5^{4-}$ or $Na_4Fe_2O_5$ is stable in contact with the melt. In moderately basic media, the stable iron oxide species of FeO^{2-} or $NaFeO_2$, and in acidic media Fe_2O_3, are formed [14].

The thermodynamic calculations based on potential $p0^{2-}$ relationships suggested that the basicity of the melt increases with temperature increase [19–21], which favors incorporation of sodium in the scale.

The following electrochemical reactions were predicted [22] in the formation of various oxides on iron surface in the presence of oxide ions (0^{2-}).

$$Fe + O^{2-} = FeO + 2e^{-} \quad (11)$$

However, FeO (wustite) is stable only above 570 °C. FeO decomposes into Fe_3O_4 and, apparently, Fe_2O_3 at lower temperature as:

$$3FeO + O^{2-} = Fe_3O_4 + 2e^{-} \quad (12)$$

$$2Fe_3O_4 + O^{2-} = 3Fe_2O_3 + 2e^{-} \quad (13)$$

In the presence of oxide and sodium ions, generally $NaFeO_2$ followed by $Na_4Fe_2O_5$ may be formed as:

$$2FeO + 5O^{2-} = Fe_2O_5^{4-} + 6e^{-} \quad (14)$$

$$Fe_2O_5^{4-} = 2FeO_2^{-} + O^{2-} \quad (15)$$

$$FeO_2^{-} + Na^{+} = NaFeO_2 \quad (16)$$

$$Fe_2O_5^{4-} + 4Na+ = Na_4Fe_2O_5 \quad (17)$$

AISI 304 Results

The superficial analysis performed by SEM is shown in Fig. 14.

Traces of small crystals are observed in the surface analysis, confirmed by the EDX analysis performed in the cross section (Fig. 15b).

In the transversal study of the sample (Fig. 15a, b), a first layer of $FeCr_2O_4$ spinel is observed with an external layer of $MgFe_2O_4$.

The EDX test, performed in different zones of the oxide layer shows the evolution on wt% of the elements available on the layer, highlighting the closest layer to the base material, composed by $FeCr_2O_4$ who exert a protective effect to the steel.

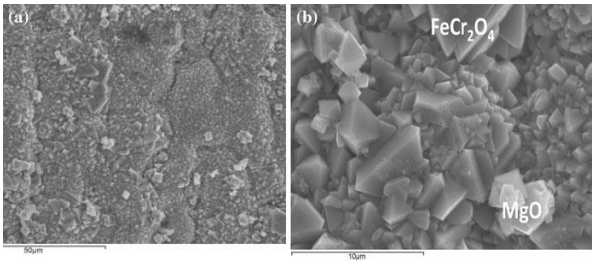

Fig. 14 a Superficial view of AISI 304 and detail and b at the end of the test

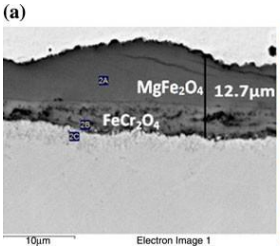

(b)

Weight %	O	Na	Mg	Cr	Mn	Fe	Ni	Mo
2A	23.54	1.31	2.99	0.78	0.84	69.48	1.06	-
2B	22.61	0.67	-	17.92	2.90	43.34	11.84	0.71
2C	2.22	-	-	16.43	0.43	67.38	13.07	0.47

Fig. 15 a Cross section of AISI 304 immersed at 550 °C in the binary salt at the end of the test and b EDX analyze

Above this layer, no diffusion of Cr is observed, noting a major contend of oxygen, iron and magnesium.

The characterization of the sample via X rays (Fig. 16) reveals the presence of a iron and chromium protective spinel and confirm the presence of the $MgFe_2O_4$.

We note also that sodium content in the outer part of the layer is due to the formation of Na_2CO_3.

High temperature corrosion test have being carried out in an open furnace allowing the addition of atmospheric CO_2, liable to forming some carbonate species in a reaction bulk.

Kramer et al. [23] have been studied the reactions of decomposition of nitrates, as well as the addition of CO_2:

$$2NaNO_3 \rightarrow Na_2O + 5/2O_2 + N_2 \quad (19)$$

$$2NaNO_3 + CO_2 \rightarrow Na_2CO_3 + N_2 + 5/2O_2 \quad (20)$$

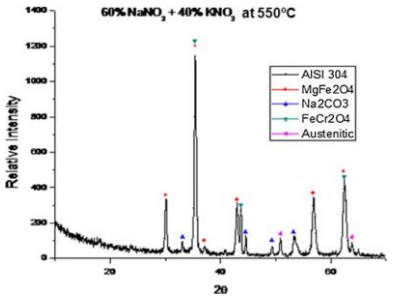

Fig. 16 DRX of AISI 304 stainless steel after 2,000 h of test

Alternatively, carbon dioxide may react with alkali metal oxides as in Reaction 21:

$$Na_2O + CO_2 \rightarrow Na_2CO_3 \quad (21)$$

These sodium carbonates are insoluble products on the salt which are deposited on the substrate surface in contact with these mixtures.

AISI 430 Results

The superficial test performed by SEM is shown in Fig. 17.

As show on weight gain (Fig. 11), AISI 430 steel presents poor behaviour against the corrosion at 550 °C in 60 % $NaNO_3$ + 40 % KNO_3 mixture.

Cross section AISI 430 steel (Fig. 18a) shows a heavy corrosion, reaching a maximum layer thickness of 138.5 lm.

As show in the results of the EDX analysis (Fig. 18b), a percent of Cr diffuse from the material, but in this case, there is not formation of the $FeCr_2O_4$ protective layer, reaching major quantities of iron and oxygen. As show in Fig. 18a the formed oxide layer shows a laminated appearance, weak and non protective.

The layer is delineated by porosity or cracks and the EDX analyze reveals that each band appears to be partitioned into alternating layers consisting of Cr-rich and Cr-poor iron oxide. This behavior varies from the austenitic alloy, where we found a well shaped protective layer as shown in Fig. 15.

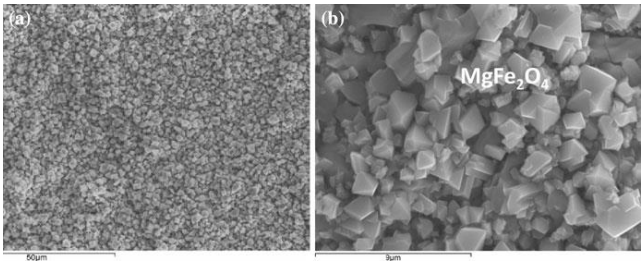

Fig. 17 a Superficial view of AISI 430 and detail and b at the end of the test

(a)

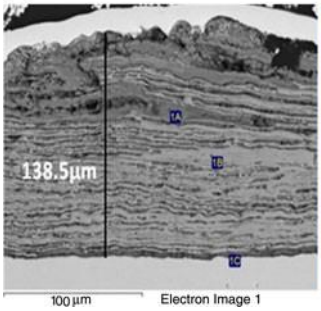

(b)

Weight%	O	Na	P	Ca	Cr	Fe	Ni
1A	22.67	2.83	25.14	0.30	-	44.69	4.36
1B	20.53	0.64	-	-	7.04	71.35	0.44
1C	13.81	1.71	16.07	1.37	7.15	55.65	4.24

Fig. 18 a Cross section of AISI 430 immersed at 550 °C in the binary salt at the end of the test and b EDX analyze

The most probable reason whereby the detected spinel not appear to be protective, may be due to fact that the ferritic steel shows preferential channels for arrange the chromium diffusion in located zones of the material. However, in austenitic steel, the diffusion of Cr occurs along the entire material, showing a uniform layer.

These corrosion products are confirmed via DRX (Fig. 19) like hematite, $MgFe_2O_4$ and a small quantity of $FeCr_2O_4$ spinel.

It has been shown in this research, according with bibliography [24], that magnesium from these impurities form stable compounds in the nitrates reactivity in terms of magnesium oxides or entering into the structure of magnetite (Fe_3O_4) to form $MgFe_2O_4$ spinel, also in processes with a more severe corrosion.

Chemical Analyzes

At the same time, several tests were arranged on the salt mixture containing the steels, before and after 2,000 h trials, observed in Table 3.

The importance of the studied remaining parameters resides in the following facts:

- Cl^-: Appears as a corrosion enhancing agent. A slightly increase comparing with initial value is related with a decomposition reaction of the perchlorate within the mixtures (Reaction 22).
- SO_4^{2-}: Important parameter to follow due to the fact that sulphates are able to form insoluble compounds which can cause clogging of pumps and pipes for the fact of the circulation of salt in the solar power plant.

Table 3 Analysis of salts before and after the corrosion test

60 % $NaNO_3$ + 40 % KNO_3	Initial values	AISI 304	AISI 430	T22
Cl (%)	0.2863	0.36	0.30	0.35
SO_4^{2-} (lg/g)	1044.6	3,194	1,201	1,662
Cr (lg/g)	\ 1	12	107	120
Fe (lg/g)	3.42	4.1	4.8	17
Mg (lg/g)	455.2	374	171	536

- Cr and Fe percents can introduce the idea of the scope of the corrosion in the material for the release of the compounds within the salt.
- Mg is an important impurity in the salt that form oxides and is able to endorse the hematite structure.

Analyze reveals a significant increasing of Cl^- on salt mixture. The reason of this increment is in Reaction 22:

$$ClO_4^- \rightarrow 2O_2 + Cl^- \quad (22)$$

When the temperature increases, the perchlorate ion starts to being dissociated into oxygen and chloride, which raise exponentially the process of corrosion of materials in contact with this environment. The values of perchlorate (ClO_4^-) can be reduced by increasing the values of chlorides in the melt [14]. Is important to point out that perchlorate ion is an impurity presented on commercial salts used in this research.

The free energy change for perchlorate reduction is favorable based on the data available for low temperature and can also be reduced by other impurities in the molten salt. The stability of perchlorate have been reported to be stable in KNO_3 at 450 °C [26], whereby at 550 °C is an important parameter to control, since O_2 and Cl^- can be released and they are corrosion enhancing agents.

The results on Table 3 shows that the amount of Cl^- in the salt at the end of the test is slightly higher to the initial values where we can conclude that some amount of perchlorate ion is decomposing although those values do not represent a big influence in the corrosion process.

Some other results can be highlight like the rising of Cr and Fe values on salt mixture depending of the corrosion extend on steel when the layers are riding from metal surface.

This result explains the worst behaviour of the ferritic steel AISI 430 comparing with the austenitic AISI 304, as we can note in the test performed on the salt at the end of the experimental procedure, where we obtain high values of Cr (107 lg/g), noting the lost of the stainless properties.

Is also remarkable the high content of iron noted on the salt in contact with the material T22 due to the high percent of corrosion in this material that provides that formed oxide it spreads to the salt.

Conclusions

This research performs a complete thermal study in the commercial grade of the solar salt, currently used like storage material in concentrated solar power (CSP) plants, evaluating melting points, phase transition, heat capacity, thermal decom- position by DSC and TGA.